

# Does HESS J1731-347 have a thick crust ?

Sebastian Kubis<sup>1,\*</sup> and Włodzimierz Wójcik<sup>1</sup>

<sup>1</sup>*Department of Physics, Cracow University of Technology, Podchorążych 1, 30-084 Kraków, Poland*

A relativistic mean-field model with a crossing term of isovector-scalar and isoscalar mesons, the Cracow crossing terms (CCT) model, has previously been shown to be capable of explaining the light and compact object HESS J1731-347. Here, the model is supplemented with a correct treatment of the phase transition. Applying the thermodynamically consistent Gibbs conditions shows that a mixed-phase system occurs in the core of the neutron star over a wide range of densities, extending up to the neutron star crust, leading to an intriguing stellar structure with a thick and massive crust.

## I. INTRODUCTION

The supernova remnant HESS J1731-347 [1] appears to contain a neutron star (NS) with an intriguingly compact size (radius around 10 km) and low mass (around  $0.8 M_{\odot}$ ). It is expected that a low-mass star would have a larger radius because of its weaker gravity. Such a compact size for a low-mass NS may only be explained by a rather specific equation of state (EOS). This EOS must describe matter that is soft at low densities (around saturation density,  $n_0$ ) and stiffens rapidly as the density increases to support the existence of a star with mass above  $2 M_{\odot}$ , in line with the well-constrained observation of the most massive NS (PSR J0740+6620 [3]) at  $2.08 \pm 0.07 M_{\odot}$ . This leads to a characteristic Z shape in the mass–radius relation, with lower-mass stars being more compact.

Many models of compact stars have been proposed to explain HESS J1731-347. Most involve exotic components that are responsible for softening the EOS, like kaon condensation [2] or strange quark matter [4], which lead to a hybrid star. The EOS softening may be a result of a phase transition, regardless of the type of matter in which it occurs. A general analysis of that kind was presented in [5]. Exotic components may explain the compact size of HESS J1731-347, but these approaches do not generally align well with other mass–radius measurements or estimates based on gravitational wave detection.

Some authors have instead attempted to revise the standard nuclear models, without introducing exotic components. A promising idea was to include meson crossing terms in the relativistic mean-field theory. The scalar-meson  $\sigma$ – $\delta$  crossing term, introduced in [6], leads to a soft EOS at low densities. The idea of a scalar-meson crossing term together with vector mesons was later considered in [7, 9]. Many meson crossing terms were thoroughly explored in [10]. Thanks to these works, one may conclude that the inclusion of vector meson crossing terms eliminates the desired softening of matter at low densities.

Another valuable class of approaches is the density-dependent relativistic mean-field (DD-RMF) models.

In [8], with a Bayesian analysis, it was shown that DD-RMF models without meson crossing terms cannot agree with HESS J1731-347 and other observational constraints. Additionally, nonstandard explanations for HESS J1731-347 have been proposed, like a neutron star with a dark matter component [12] and extended gravity, in which the standard Tolman–Oppenheimer–Volkoff equations take a different form [13].

In [11], a nuclear model was proposed, which has an EOS with the required properties and can accommodate low-mass and compact objects like HESS J1731-347 alongside other mass–radius constraints from observations. In this model, the dense matter undergoes a phase transition at a density slightly above the saturation point. To obtain a unique pressure–density relation, the commonly used Maxwell construction was employed. It is well known that the Maxwell construction is not quite correct for nuclear matter with leptons. It was discussed thoroughly in [14] that for systems with two conserved quantum numbers, charge and baryon number, the Maxwell construction cannot ensure chemical equilibrium for the two separated phases. The pressure and chemical potentials for all particle species  $i$  present in both phases, denoted by  $I$  and  $II$ , must be the same:

$$P^{(I)} = P^{(II)}, \quad \mu_i^{(I)} = \mu_i^{(II)} \quad (1)$$

The Maxwell construction, also applied in [11], is based on the assumption that neutron–proton–lepton ( $npl$ ) matter is locally neutral. Under this constraint, we cannot ensure that all the Gibbs conditions are satisfied. The *equal-area* rule, in the case of  $npl$  matter, breaks the equality of chemical potentials for all charged particles, that is,  $\mu_p, \mu_e$ , and  $\mu_{\mu}$ .

In this work, we use the so-called Gibbs construction, in which the proper conditions for the two-phase system are fulfilled. It is found that the matter undergoes a phase separation, with one phase free of protons. This coexistence of an  $npl$  phase with a neutron–lepton ( $nl$ ) phase spans a broad range of densities, from a moderate NS core density down to the deep inner crust region. This means that the NS crust is thicker and makes a substantially greater contribution to the total stellar mass and moment of inertia than in typical approaches. Our aim is to present this intriguing NS structure and investigate possible observational consequences.

\* skubis@pk.edu.pl

## II. THE RELATIVISTIC MEAN-FIELD MODEL

The Cracow crossing terms (CCT) model of nuclear interaction proposed in [11] is based on a relativistic Lagrangian with a standard kinetic term and interaction terms:

$$\mathcal{L} = \mathcal{L}_{\text{kin}} + \mathcal{L}_{N\phi} + \mathcal{L}_{\text{cross}}, \quad \phi = \sigma, \omega, \rho, \delta. \quad (2)$$

It uses four types of meson fields,  $\phi = \sigma, \omega, \rho, \delta$ , which are linearly coupled to all nucleonic currents admissible by the isospin symmetry:

$$\mathcal{L}_{N\phi} = g_\sigma \sigma \bar{\psi} \psi - g_\omega \omega_\mu \bar{\psi} \gamma^\mu \psi - \frac{1}{2} g_\rho \vec{\rho}_\mu \bar{\psi} \gamma^\mu \vec{\tau} \psi + g_\delta \vec{\delta} \bar{\psi} \vec{\tau} \psi - U(\sigma), \quad (3)$$

where

$$U(\sigma) = \frac{1}{3} b m (g_\sigma \sigma)^3 + \frac{1}{4} c (g_\sigma \sigma)^4 \quad (4)$$

is the self-interaction of the  $\sigma$  meson. The key ingredients of the model are the meson-meson interaction terms (crossing terms), in which the scalar-isovector field  $\vec{\delta}$  is coupled to the two isoscalar fields,  $\sigma$  and  $\omega$ :

$$\mathcal{L}_{\text{cross}} = \frac{1}{2} g_{\sigma\delta} \sigma^2 \vec{\delta}^2 + \frac{1}{2} g_{\omega\delta} \omega_\mu \omega^\mu \vec{\delta}^2, \quad (5)$$

In the spirit of the relativistic mean-field approach, the meson fields contribute to the total energy through their average values, which can then be replaced by the effective masses of nucleons:

$$m_p = m - g_\sigma \bar{\sigma} - g_\delta \bar{\delta}^{(3)}, \quad (6)$$

$$m_n = m - g_\sigma \bar{\sigma} + g_\delta \bar{\delta}^{(3)}, \quad (7)$$

where  $m$  is the bare nucleon mass.

The energy density for nucleonic matter can be expressed in terms of the nucleon scalar  $n_i^s$  and vector  $n_i$  densities and effective masses, which are functions of the densities  $m_i(n_p, n_n)$ , for  $i = p, n$ :

$$\begin{aligned} \varepsilon_{\text{nuc}} = & \sum_{i=p,n} \frac{1}{4} (3E_{F,i} n_i + m_i n_i^s) + \frac{1}{2C_\sigma^2} (m - \bar{m})^2 \\ & + \frac{C_\omega^2}{2} \frac{n^2}{1 + C_\omega^2 \Lambda_{\omega\delta} (\Delta m / 2)^2} + \frac{C_\rho^2}{8} (2x - 1)^2 n^2 \\ & + \frac{\Delta m^2}{8C_\delta^2} + \frac{1}{8} \Lambda_{\sigma\delta} (m - \bar{m})^2 \Delta m^2 + U(m - \bar{m}), \end{aligned} \quad (8)$$

where  $\Delta m = m_n - m_p$  and  $\bar{m} = (m_n + m_p)/2$ . Similarly, the pressure is

$$\begin{aligned} P_{\text{nuc}} = & \sum_{i=n,p} \frac{1}{4} (n_i E_{F,i} - m_i n_i^s) - \frac{(m - \bar{m})^2}{2C_\sigma^2} \\ & + \frac{C_\omega^2 n^2}{2(\frac{1}{4} C_\omega^2 \Delta m^2 \Lambda_{\omega\delta} + 1)} + \frac{1}{8} C_\rho^2 n^2 (1 - 2x)^2 \\ & - \frac{\Delta m^2}{8C_\delta^2} + \frac{1}{8} \Delta m^2 \Lambda_{\sigma\delta} (m - \bar{m})^2 - U(m - \bar{m}) \end{aligned} \quad (9)$$

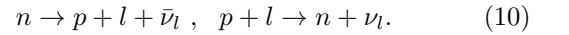
TABLE I. Coupling constants for three CCT models with  $L = 40$  MeV and different values of  $C_\sigma^2$ .

$C_\sigma^2$ (fm <sup>2</sup> )	$C_\omega^2$ (fm <sup>2</sup> )	$b$ (-)	$c$ (-)	$C_\rho^2$ (fm <sup>2</sup> )	$C_\delta^2$ (fm <sup>2</sup> )
12	6.9769	0.004733	-0.0052878	15.2938	2.63799
13	7.9531	0.003695	-0.0045224	13.9852	2.33674
14	8.9055	0.003005	-0.0039370	12.9888	2.11461

with a typical negative contribution from scalar mesons. In the expressions for the energy density and pressure, it is more convenient to introduce coupling constants different from those appearing in the Lagrangian:  $C_i = g_i/m_i$ ,  $\Lambda_{\sigma\delta} = g_{\sigma\delta}/g_\sigma^2 g_\delta^2$ , and  $\Lambda_{\omega\delta} = g_{\omega\delta}/g_\omega^2 g_\delta^2$ . Together with  $b$  and  $c$  in the  $U(\sigma)$  potential, they are independent parameters which uniquely define the model. Their values come from fitting to the basic properties of matter at the saturation point density  $n_0 = 0.16$  fm<sup>-3</sup>. In [11], it was shown that a compact low-mass NS is attained only for low values of the symmetry energy slope  $L$ . Here, we adopt the value  $L = 40$  MeV. Table I presents parameters for three models with this value that differ in their stiffness at higher densities. The stiffness of the EOS at higher densities is crucial to provide a sufficiently high maximum mass of the NS. In our model, this property is controlled by the value of  $C_\sigma^2$ . A wider discussion of model parametrization and its connection to experimental data is presented in our previous works [6] and [11].

## III. PHASE SEPARATION

In addition to nucleons, the NS matter contains the leptons  $e$  and  $\mu$ , which are produced in the following beta processes:



The lepton contributions to the total energy and pressure are given by standard expressions that depend only on the lepton chemical potentials  $\varepsilon_i(\mu_i)$  and  $P_i(\mu_i)$ , for  $i = e, \mu$ . As discussed in [11], for low values of  $L$ , the  $np$  matter becomes unstable with respect to charge fluctuations and undergoes a phase transition. The quantity that indicates the instability of the matter is its incompressibility under a constant chemical potential:

$$K_\mu = \left( \frac{\partial P}{\partial n} \right)_\mu > 0. \quad (11)$$

In the region of densities where this condition is violated, the matter cannot stay as a one-phase system; it must split into two coexisting phases with different charge and baryon densities. The coexistence conditions (1) require the equality of chemical potentials (chemical equilibrium) and pressures (mechanical equilibrium) between those

two phases. Usually, the NS matter remains in beta equilibrium at all densities. The temperature of NS matter can be on the order of millions of kelvins and is negligible in comparison to the chemical potentials,  $k_B T \ll \mu_i$ , but this means that the energy levels around the Fermi energies (the Fermi energy is here equal to the chemical potential) are not completely occupied. So, the particles may exchange their energy via the beta reactions (10), which leads to the following relation between chemical potentials for the degenerate fermions:

$$\mu_l = \mu_n - \mu_p. \quad (12)$$

The chemical potential  $\mu_\nu$  is absent here, as the weakly interacting neutrinos escape from the system, carrying away thermal energy on the order of  $k_B T$ . The symmetry energy  $E_s$  uniquely determines the proton fraction  $x$  and the lepton abundance through the relation

$$\mu_n - \mu_p = 4(1 - 2x)E_s. \quad (13)$$

Thus, when  $E_s(n) \leq 0$ , lepton production is blocked and the nucleonic matter contains only neutrons. However, the pure neutron phase may also appear for  $E_s(n) > 0$  as a consequence of the Gibbs conditions for a two-phase system. When the symmetry energy is low but still positive, it may occur that one of the phases (with the lower density) cannot contain protons, because the difference between neutron and lepton energies is too small to produce protons:

$$\mu_n^I - \mu_l^I < \mu_p^I. \quad (14)$$

Such a behavior was discussed in [16]. This is a mechanism analogous to the neutron drip phenomenon occurring in the inner crust of the NS. In our model, it appears that the Gibbs conditions are satisfied for neutrons and electrons but not for protons:

$$\mu_n^I = \mu_n^{II}, \quad \mu_l^I = \mu_l^{II}, \quad \mu_p^I > \mu_p^{II}. \quad (15)$$

Protons are confined to the  $II$  phase as they have lower energy there.

Summarizing, the system consists of two phases: a low-density phase ( $I$ ) with neutrons and leptons and a high-density phase ( $II$ ) containing neutrons, protons, and leptons. The  $I$  phase is negatively charged, whereas the  $II$  phase is positively charged. The phases must fill the space in the following ratio to ensure the global neutrality of the dense matter:

$$-w(n_e^I + n_\mu^I) + (1 - w)(n_p^{II} - n_e^{II} - n_\mu^{II}) = 0 \quad (16)$$

where  $w = V^I/V$  is the low-density volume fraction and  $V = V^I + V^{II}$  is the total volume of the system. Figure 1 shows the phase diagram of the nucleon-lepton matter. The light-blue line represents the proton fraction  $x_\beta$  for a homogeneous, one-phase system under beta equilibrium that is charge neutral. This neutrality line marks the border between positively charged matter (all  $(n, x)$  points

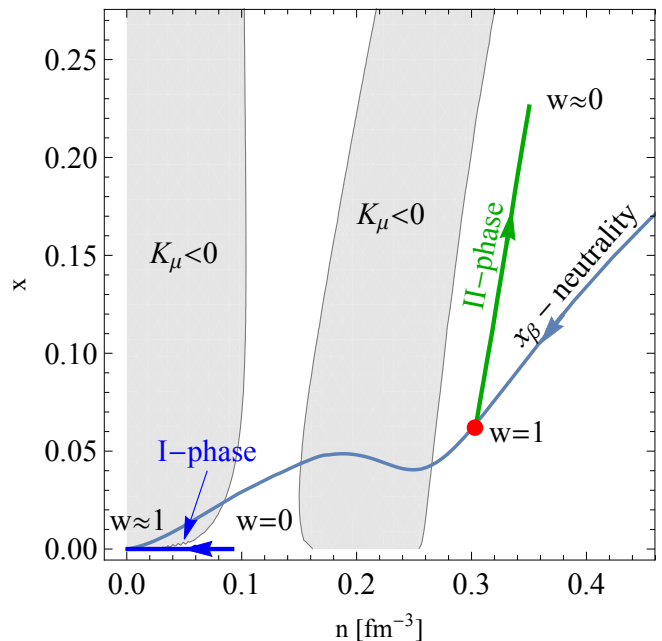


FIG. 1. Phase coexistence diagram for the model with  $C_\sigma^2 = 12$  and  $L = 40$ . The gray regions correspond to  $K_\mu < 0$ . Blue and green lines depict  $I$  and  $II$  phases, respectively, with the limiting values of  $w$ . The red point indicates the place where the homogeneous phase vanishes in favor of the two-phase system.

above) and negatively charged matter (below). The neutrality line passes through unstable regions  $K_\mu < 0$ , so it cannot represent a physical system. Going from high densities, where neutral matter is stable, at some density around  $0.3 \text{ fm}^{-3}$ , the system splits into two phases, which are depicted by blue and green lines. The proton-neutron phase ( $II$ ) fades in favor of the neutron phase ( $I$ ), as  $w \rightarrow 1$ ; however, the  $I$ -phase never fills the entire space, even for low densities. Therefore, at low densities,  $w$  is only approximately equal to zero.

The average baryon number density of the two-phase system is given by

$$\bar{n} = w n^I + (1 - w)n^{II}, \quad (17)$$

and so the energy of the two-phase system is the weighted sum of both phases:

$$\bar{\varepsilon} = w \varepsilon^I + (1 - w)\varepsilon^{II}. \quad (18)$$

Figure 2 shows the energy of the two-phase system and that of homogeneous,  $\beta$ -equilibrated matter for three different models. It confirms that the two-phase system is the preferred state of matter at all densities below  $n \approx 0.3 \text{ fm}^{-3}$ . A similar two-phase system appearing at densities slightly above  $n_0$  was analyzed in [17], but there, the two-phase system disappeared close to  $n_0$  and  $npl$  matter was again homogeneous. Here, the two-phase matter persists down to all densities below  $n_0$ . The residual proton-neutron phase may be interpreted

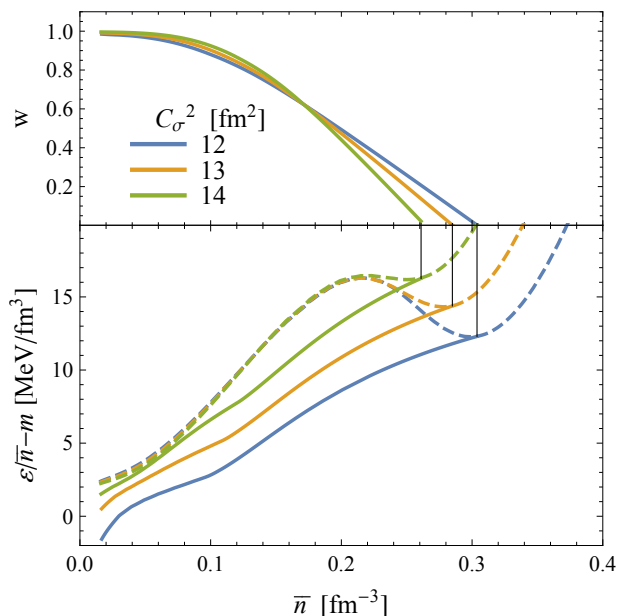


FIG. 2. Lower plot: energy difference between homogeneous matter and the two-phase system. Upper plot: volume fraction of the  $I$  phase.

as quasi-nuclei sparsely placed in the region dominated by neutron fluid; such a system corresponds to the inner crust structure. So, in our model, the crust–core transition moves up to a density around  $0.3 \text{ fm}^{-3}$ . This is much higher than the typical crust–core transition point, which, depending on the nuclear model, fluctuates in the range between  $0.03$  and  $0.08 \text{ fm}^{-3}$ . In this work, we do not include finite-size effects coming from surface or Coulomb energies, which are essential in determining the size of structures (droplets, rods, etc.) for a mixed-phase system. The surface and Coulomb energies depend on the density difference between phases [14], which goes to zero at the splitting point, so including these effects does not change the conclusion about the density reached by the two-phase system. Table II lists the critical density values for two-phase system formation. The density decreases slightly as the strength of  $C_\sigma^2$  coupling increases.

TABLE II. Values of the critical density for two-phase system formation for three different models.

$C_\sigma^2$ ( $\text{fm}^2$ )	12	13	14
$n_{2\text{ph}}$ ( $\text{fm}^{-3}$ )	0.3038	0.2849	0.2610
$n_{\text{join}}$ ( $\text{fm}^{-3}$ )	0.0025	0.0656	0.0656

To obtain a complete model of an NS, the EOS for the NS crust must be joined with the EOS of our model. Here, to model the crust, we use the SLy4 EOS [15]. At densities below  $n_0$ , the pressure in our model is smaller than for Sly4, but at a density on the order of  $10^{-2} \text{ fm}^{-3}$ , there is a point where the two pressures are equal; this

is where the EOSs are joined. The joining densities  $n_{\text{join}}$  are given in Table II.

The EOSs for all three  $C_\sigma^2$  values are shown in Fig. 3. For comparison, the EOSs based on the Maxwell construction are shown with dashed lines. One may notice that the Gibbs construction substantially alters the pressure–density relation. Especially for the model with  $C_\sigma^2 = 12$ , the EOS is much softer at low densities. In Fig. 3, a plot with the speed of sound, defined as  $v_s^2 = \left(\frac{\partial P}{\partial \rho}\right)_q$ , is also shown. The dashed lines extend into the unphysical region where  $v_s$  vanishes; a vanishing speed of sound leads to a discontinuity in the density profile of an NS. The solid lines, corresponding to the Gibbs construction, indicate small but finite values of  $v_s$  at lower densities, which rapidly increase and even exceed the limit  $v_s < c/\sqrt{3}$  from the EOS for free ultrarelativistic fermions [18]. Various limits for  $v_s$  were discussed recently in [5]; it was shown that the  $c/\sqrt{3}$  limit must be broken if the nuclear EOS is to explain HESS J1731-347 observations and the fact that  $M_{\text{max}}$  for an NS is above  $2 M_\odot$ . The values of  $v_s$  obtained here are in agreement with the more general condition:

$$v_s < \frac{\varepsilon - 1/3P}{\varepsilon + P}, \quad (19)$$

which is valid for any  $P(\varepsilon)$  and comes from relativistic kinetic theory [19].

The key finding of this section is that a nuclear model with a correct chemical equilibrium condition for the two-phase system leads to a thick NS crust. A similar scenario, in which a pure neutron phase coexists with an

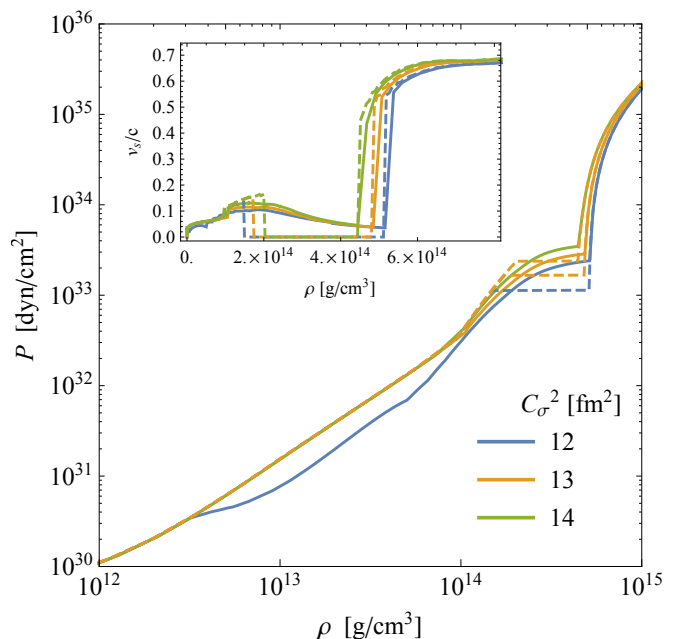


FIG. 3. Plots of EOSs for three models. The dashed lines represent EOSs based on the Maxwell construction.

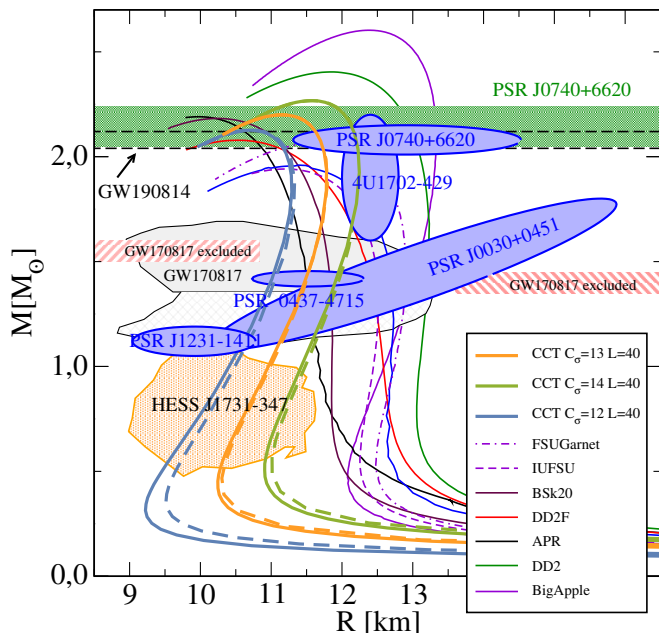


FIG. 4. Mass–radius relation for CCT models. Some other nuclear models are included for comparison.

*npl* phase, was considered in [17], but there, the two-phase system occurs at densities approximately between  $0.1 \text{ fm}^{-3}$  and  $0.3 \text{ fm}^{-3}$ , corresponding to the outer core region. Here, the two-phase system extends to much lower densities, up to the contact with the inner crust. It seems natural to conclude that in this case, the NS crust extends to much deeper regions of the star. In the next section, we consider the implications for NS observables.

#### IV. NEUTRON STAR PROPERTIES

In this section, the most relevant NS properties are discussed with respect to the inclusion of Gibbs conditions. In Fig. 4, the mass–radius relation is shown. The solid lines correspond to the Gibbs EOS and the dashed lines to the Maxwell construction. As discussed above, the Gibbs construction softens the EOS at low densities, making low-mass stars more compact. The solid lines move to smaller values of  $R$ , and the desired Z-like relation is more pronounced. Although the Gibbs construction significantly alters the pressure–density relation at lower densities, it does not have a visible effect for stars with higher masses. The maximum mass is almost the same as in the Maxwell construction case. For reference, the mass–radius relations of other nuclear models are also shown. The names of the models are listed in the legend: APR [20], DD2, DD2F [21], BSK20 [22], FSUGarnet, IUFSU, and BigApple [23]. The latter three are relativistic mean-field models similar to the one introduced in this work.

In Fig. 4, the observational results are also shown. The 68% confidence level of the mass–radius measure-

ment for HESS J1731-347 is indicated by the orange region. The blue elliptical regions correspond to the most accurate NICER measurements of the objects PSR 0740+6620 [24], PSR J0030+0451 [25], and PSR J0437-4715 [26]. The recent result for PSR J1231-1411 [27] is also included, but we mention that it is debated due to the earlier analysis [28]. We also include the mass and radius estimates from X-ray bursts from an accreting NS in 4U 1702-429, presented in [29].

The interval for the lower bound for the maximum mass, derived from precise Shapiro delay measurements for PSR J0740+6620, is indicated by the green region. The gray regions correspond to the two estimated masses of the components of the binary system that merged and produced gravitational waves in the event GW170817. The black dashed lines mark a lower-bound interval for the lower component of the event GW190814 under the assumption that it was a rapidly spinning NS [30]. The red dashed regions correspond to estimated excluded regions from the analysis of the GW170817 event [31, 32].

All three models, with  $C_\sigma^2 = 12, 13, 14 \text{ fm}^2$ , fulfill observational constraints, although the model with  $C_\sigma^2 = 14 \text{ fm}^2$  is in better agreement with the lower bound for the maximum NS mass based on the pulsar J0740+6620. The only problematic object is PSR J1231-1411. This is as compact as HESS J1731-347 and has a mass even larger. As discussed above, such a small radius is sensitive to the assumptions concerning the hotspot shape and NS atmosphere modeling [27, 28].

Finally, we describe the main crustal properties in the CCT model. Applying the Gibbs conditions to the two-phase system that appears in our model reveals that the NS crust may encompass a much wider range of densities than in most models. If  $n_{2ph}$  is treated as the crust–core transition density, the NS crust reaches up to approximately  $2n_0$  (see Table II). This means that the crustal contribution to the stellar parameters is much more pronounced. In Fig. 5, the crust thickness  $\Delta R$  and its contribution to the stellar mass and moment of inertia are shown. The dashed line indicates the crustal parameters derived from the CCT model with the Maxwell construction, which was used in [11], where the crust–core transition was at around  $n_{cc} = 0.056 \text{ fm}^{-2}$ . Their behavior does not diverge substantially from most of the other models, but the values obtained with the Gibbs construction are considerably different. It is interesting that for the case of HESS J1731-347, the crust is about 50% thicker and its mass and moment of inertia several times larger than in standard crust models. Such a large contribution to the crustal parameters should significantly alter the thermal evolution of the object and its rotational properties.

#### V. CONCLUSIONS

We have shown that using the thermodynamically consistent Gibbs construction for the first-order phase transition that occurs in the relativistic mean-field model with

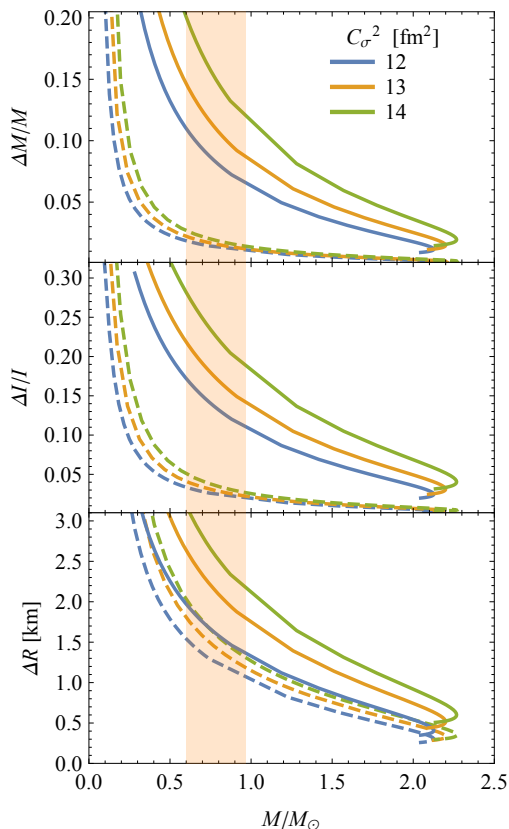


FIG. 5. Crustal fraction of mass, moment of inertia, and radius. The orange shaded region indicates the HESS J1731-347 mass measurement.

$\sigma$ - $\delta$  and  $\omega$ - $\delta$  meson crossing term leads to a thick neutron crust. The mass-radius relation may be controlled to some extent by the coupling to the  $\sigma$  field, and in a reasonable range of its values, the mass-radius relation is in close agreement with the most reliable observational constraints.

- 
- [1] V. Doroshenko, V. Suleimanov, G. Pühlhofer, and A. Santangelo, *Nat. Astron.* **6**, 1444 (2022).
- [2] M. Veselsky, P. S. Koliogiannis, V. Petousis, J. Leja, and C. C. Moustakidis, *Phys. Lett. B* **860**, 139185 (2025).
- [3] E. Fonseca, H. T. Cromartie, T. T. Pennucci, P. S. Ray, A. Y. Kirichenko, S. M. Ransom, P. B. Demorest, I. H. Stairs, Z. Arzoumanian, L. Guillemot, *et al. Astrophys. J. Lett.* **915** (1), L12 (2021).
- [4] P. Laskos-Patkos, P. S. Koliogiannis, and C. C. Moustakidis, *Phys. Rev. D* **109** (6), 063017 (2024).
- [5] P. Laskos-Patkos, G. A. Lalazissis, S. Wang, J. Meng, P. Ring, and C. C. Moustakidis, *Phys. Rev. C* **111** (2), 025801 (2025).
- [6] N. Zabari, S. Kubis, and W. Wójcik, *Phys. Rev. C* **99**, 035209 (2019).
- [7] T. Miyatsu, M. K. Cheoun, and K. Saito, *Astrophys. J.* **929**, 82 (2022).
- [8] C. J. Xia, W. J. Xie, and M. Bakhiet, *Phys. Rev. D* **110** (11), 114009 (2024).
- [9] F. Li, B. J. Cai, Y. Zhou, W. Z. Jiang, and L. W. Chen, *Astrophys. J.* **929** (2), 183 (2022).
- [10] T. Miyatsu, M. K. Cheoun, K. Kim, and K. Saito, *Front. Phys.* **12**, 1531475 (2024).
- [11] S. Kubis, W. Wójcik, D. A. Castillo, and N. Zabari, *Phys. Rev. C* **108** (4), 045803 (2023).
- [12] B. Hong and Z. Ren, *Phys. Rev. D* **109** (2), 023002 (2024).
- [13] E. Lope-Oter and A. Wojnar, *J. Cosmol. Astropart. Phys.* **01**, 054 (2025).
- [14] N. K. Glendenning, *Compact Stars: Nuclear Physics, Particle Physics, and General Relativity* (Springer-Verlag, New York, 1997).
- [15] F. Douchin and P. Haensel, *Astron. Astrophys.* **380**, 151 (2001).
- [16] S. Kubis, *Acta Phys. Polon. B* **38**, 3879 (2007).
- [17] S. Kubis, W. Wójcik, and N. Zabari, *Phys. Rev. C* **102**, 065803 (2020).
- [18] P. Bedaque and A. W. Steiner, *Phys. Rev. Lett.* **114** (3), 031103 (2015).
- [19] T. S. Olson, *Phys. Rev. C* **63**, 015802 (2000).
- [20] A. Akmal, V. R. Pandharipande, and D. G. Ravenhall, *Phys. Rev. C* **58**, 1804 (1998).
- [21] S. Typel, *Phys. Rev. C* **89**, 064321 (2014).
- [22] N. Chamel, A. F. Fantina, J. M. Pearson, and S. Goriely, *Phys. Rev. C* **84**, 062802(R) (2011).
- [23] F. J. Fattoyev, C. J. Horowitz, J. Piekarewicz, and B. Reed, *Phys. Rev. C* **102** (6), 065805 (2020).

- [24] M. C. Miller, F. K. Lamb, A. J. Dittmann, S. Bogdanov, Z. Arzoumanian, K. C. Gendreau, S. Guillot, W. C. G. Ho, J. M. Lattimer, M. Loewenstein, *et al.* *Astrophys. J. Lett.* **918**, L28 (2021).
- [25] M. C. Miller, F. K. Lamb, A. J. Dittmann, S. Bogdanov, Z. Arzoumanian, K. C. Gendreau, S. Guillot, A. K. Harding, W. C. G. Ho, J. M. Lattimer, *et al.* *Astrophys. J. Lett.* **887**, L24 (2019).
- [26] D. Choudhury, T. Salmi, S. Vinciguerra, T. E. Riley, Y. Kini, A. L. Watts, B. Dorsman, S. Bogdanov, S. Guillot, P. S. Ray, *et al.* *Astrophys. J. Lett.* **971** (1), L20 (2024).
- [27] L. Qi, S. Zheng, J. Zhang, M. Ge, A. Li, S. N. Zhang, F. Lu, F. J. Lu, H. Peng, H. L. Peng, *et al.* *Astrophys. J.* **981** (2), 99 (2025).
- [28] T. Salmi, J. S. Deneva, P. S. Ray, A. L. Watts, D. Choudhury, Y. Kini, S. Vinciguerra, H. T. Cromartie, M. T. Wolff, Z. Arzoumanian, *et al.* *Astrophys. J.* **976** (1), 58 (2024).
- [29] J. Nättilä, M. C. Miller, A. W. Steiner, J. J. E. Kajava, V. F. Suleimanov, and J. Poutanen, *Astron. Astrophys.* **608**, A31 (2017).
- [30] E. R. Most, L. J. Papenfort, L. R. Weih, and L. Rezzolla, *Mon. Not. Roy. Astron. Soc.* **499**, L82 (2020).
- [31] A. Bauswein, O. Just, H. T. Janka, and N. Stergioulas, *Astrophys. J. Lett.* **850**, L34 (2017).
- [32] E. Annala, T. Gorda, A. Kurkela, and A. Vuorinen, *Phys. Rev. Lett.* **120**, 172703 (2018).